Supplementary Information (SI) for ChemComm.
This journal is © The Royal Society of Chemistry 2025

Electronic Supplementary Information (ESI) for Chemical Communications. This journal is (c) The Royal Society of Chemistry 2025.

Electronic Supplementary Information (ESI)

Engineering a dually-porous Li-rich carbon coated Si/SiO_x nanosphere as high-performance Li-ion battery anode

Yajun Zhu[a], Hui Zhang[a], Xiangbing Zeng[b], Tianli Han[a], Meizhou Qi[c],Wentuan Bi[c,*], Jinyun Liu[a,*]

Experimental

Preparation of SiO_2 spheres

Typically, 2 mL of ammonia was added to a mixture of 40 mL of ethanol and 8 mL of deionized water. After magnetic stirring 30 min, 1.6 mL of tetraethyl silicate was added dropwise, followed by an additional hour of continuous stirring. The sample was then collected, centrifuged for cleaning and dried in an oven at 60 ℃.

Preparation of porous Si/SiO_x spheres

The SiO_2 spheres synthesized in the previous step were mixed and milled for 10 minutes by thermal reduction of magnesium powder. Specifically, the mass ratio of SiO_2 to Mg powder was 1:2. Then, the mixture was placed in a hydrogen-argon mixed gas atmosphere and calcined at 650 ℃ for 6 h with a heating temperature rate of 5 ℃ per minute. After the calcination was completed, the sample was soaked in 3 M HCl solution for 5 h. The sample was alternately washed with HCl solution and deionized water, and dried at 60 ℃ to obtain porous Si/SiO_x spheres.

Preparation of DP Si/SiO_x@Li-C

0.1 g of the as-prepared porous Si/SiO_x spheres was dispersed in 50 mL of

deionized water, and sonicated for 10 min. Then, 1.21 g of trihydroxymethyl aminomethane was added under stirring. The pH was adjusted to 8-8.5 by HCl solution, and 60 mg of dopamine hydrochloride was added. Finally, 0.2 g of $LiNO_3$ was dissolved. The reaction was carried out for 24 h. The sample was collected and washed with deionized water and ethanol, and dried at 60 °C. The sample was calcined at 550 °C for 2 h in a nitrogen atmosphere at a heating rate of 2 °C per minute. In control experiments, lithium salt was replaced by Li_2CO_3 or LiCl during the preparation to obtain DP Si/SiO_x@Li_2CO_3-C and DP Si/SiO_x@LiCl-C, respectively. P-Si/SiO_x@C was obtained without the addition of lithium source. DP Si/SiO_x@Li-C-0.6 was prepared by increasing the thickness of carbon layer, and Si@Li-C was synthesized by using Si nanospheres purchased from Aladdin.

Characterization

Morphology of the samples were analyzed by scanning electron microscopy and transmission electron microscopy. The structure and composition were characterized by XRD (Bruner D8 Advance), XPS (ESCALAB 250), Raman spectroscopy (Renishaw, in Via) and BET analyzer (ASAP 2460). The carbon content of the samples was analyzed using thermogravimetric analysis (TGA, Setaram Labsys Evo SDT Q600).

Electrochemical tests

The active material, acetylene black and polyvinylidene fluoride were mixed with a mass ratio of 7:2:1. The mixture was dispersed in N-methylpyrrolidone. After magnetic stirring for 8 h, the slurry was uniformly coated onto the copper foil, and placed in vacuum oven at 80 ℃. Coin cells were assembled in a glove box. The electrolyte contained $LiPF_6$ with the volume ratio of ethylidene carbonate (EC) to diethyl carbonate (DEC) being 1:1. Electrochemical performance tests were conducted on the Neware battery system. CV curves and EIS spectra were measured using an electrochemical workstation (CHI 660E).

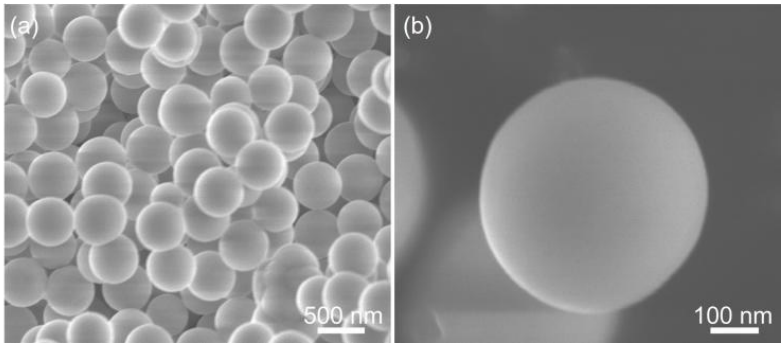

Fig. S1 (a,b) SEM images of the as-synthesized SiO_2.

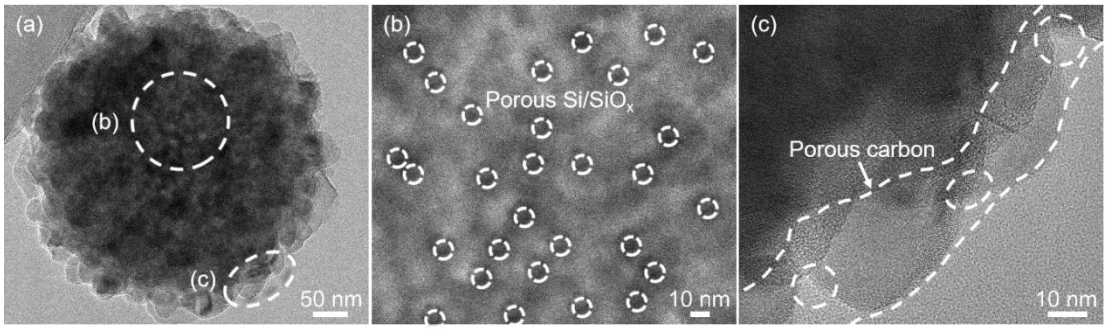

Fig. S2 TEM images of DP Si/SiO_x@Li-C: (a) individual spheres, (b) porous Si/SiO_x in the interior and (c) porous carbon layer at the edge.

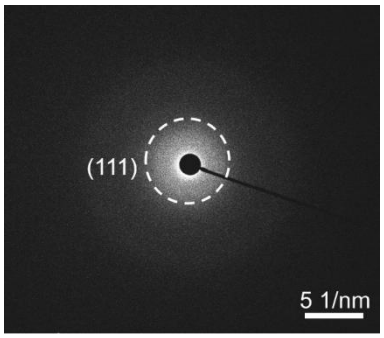

Fig. S3 SAED pattern of DP Si/SiO_x@Li-C.

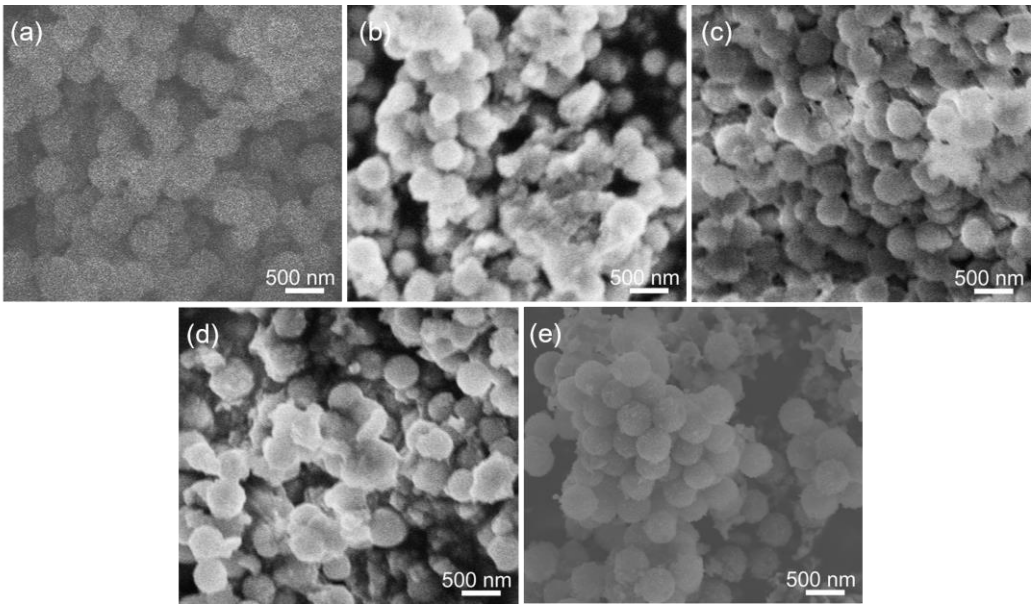

Fig. S4 SEM images of (a) Si@Li-C, (b) DP Si/SiO_x@Li-C-0.6, (c) DP Si/SiO_x@Li_2CO_3-C, (d) DP Si/SiO_x@LiCl-C, and (e) P-Si/SiO_x@C.

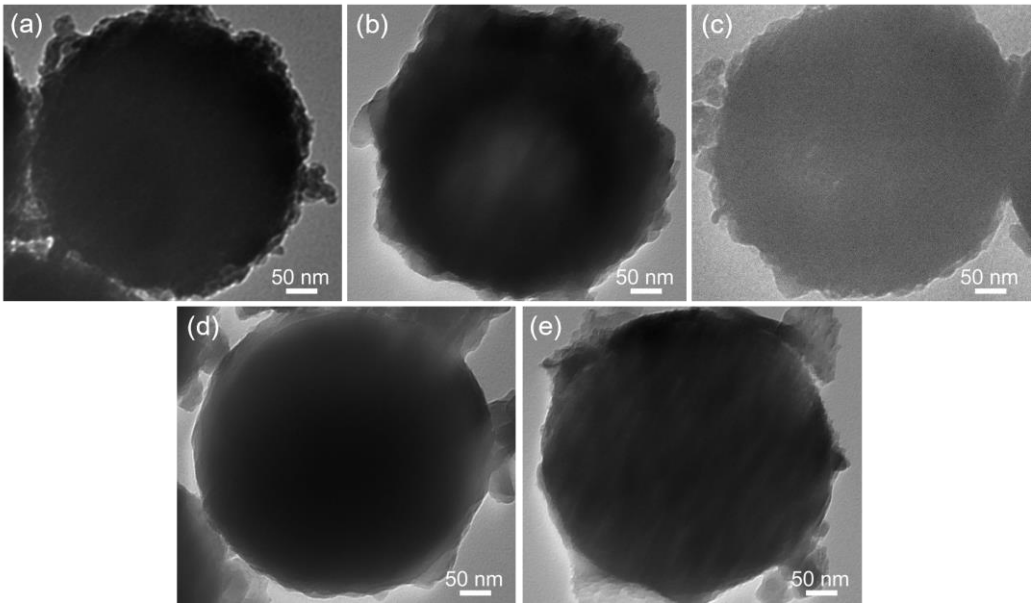

Fig. S5 TEM images of (a) Si@Li-C, (b) DP Si/SiO_x@Li-C-0.6, (c) DP Si/SiO_x@Li_2CO_3-C, (d) DP Si/SiO_x@LiCl-C, and (e) P-Si/SiO_x@C.

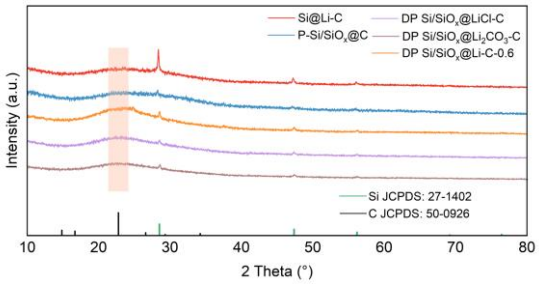

Fig. S6 XRD patterns of Si@Li-C, DP Si/SiO_x@Li-C-0.6, DP Si/SiO_x@Li_2CO_3-C, DP Si/SiO_x@LiCl-C, and P-Si/SiO_x@C.

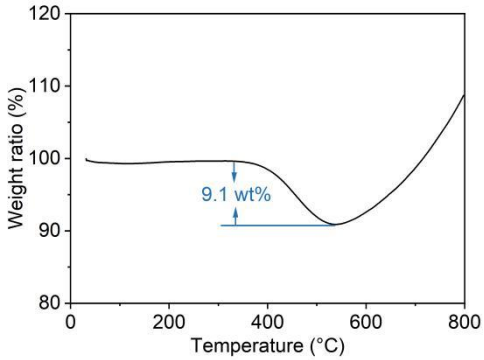

Fig. S7 TGA curve of DP Si/SiO_x@Li-C. The 9.1% mass loss between 300-550°C is ascribed to carbon decomposition, so the mass content of Si is about 1-9.1%=90.9%, indicating that the mass ratio of Si:C is 9:1 approximately since the light weight of supplied Li in the composite is non-obvious compared to Si and carbon.

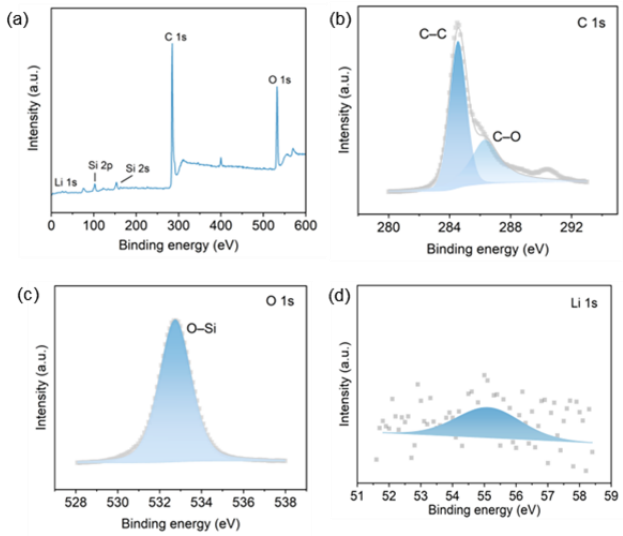

Fig. S8 XPS spectra of DP Si/SiO_x@Li-C: (a) survey spectrum, (b) C 1s, (c) O 1s, and (d) Li 1s.

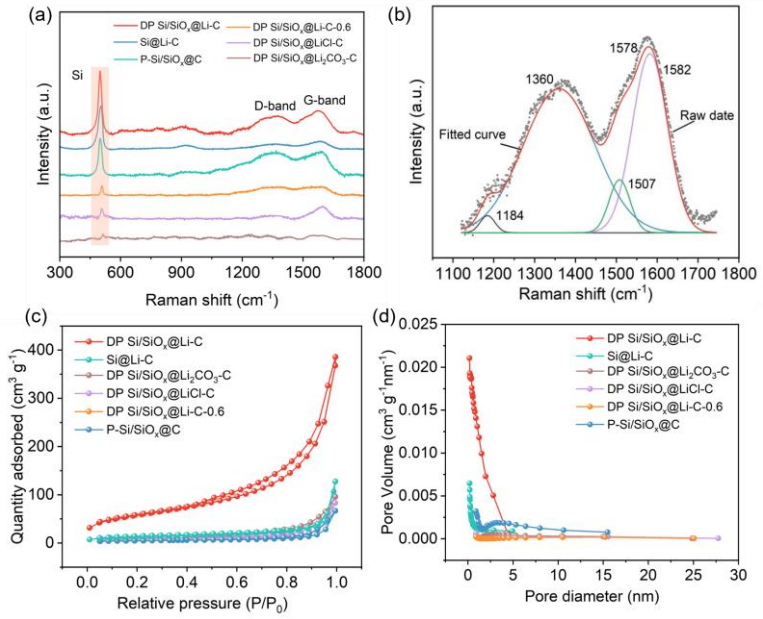

Fig. S9 (a) Raman spectra and (b) the deconvoluted spectra of DP Si/SiO_x@Li-C at the D and G bands. (c) The N_2 adsorption-desorption isotherms and (d) pore-size distribution of Si@Li-C, DP Si/SiO_x@Li-C-0.6, DP Si/SiO_x@Li_2CO_3-C, DP Si/SiO_x@LiCl-C, P-Si/SiO_x@C, and DP Si/SiO_x@Li-C.

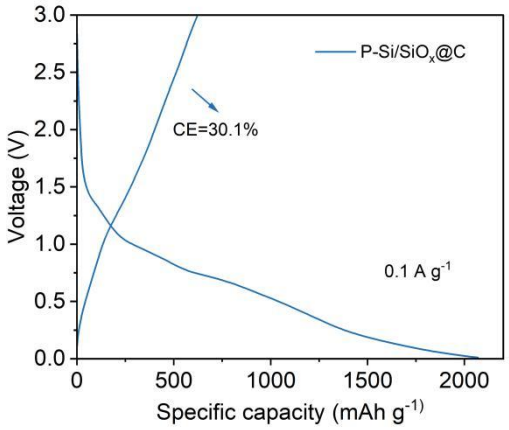

Fig. S10 First-cycle charge-discharge profile of P-Si/SiO_x@C anode at 0.1 A g^{-1}.

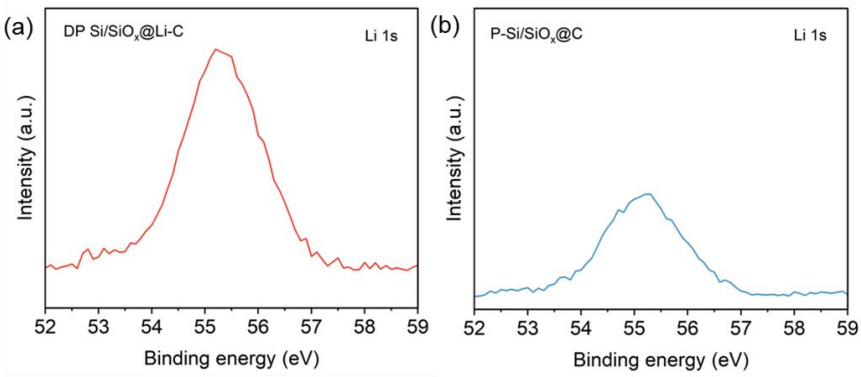

Fig. S11 XPS spectra of Li 1s in (a) DP Si/SiO_x@Li-C and (b) P-Si/SiO_x@C after the first two cycles.

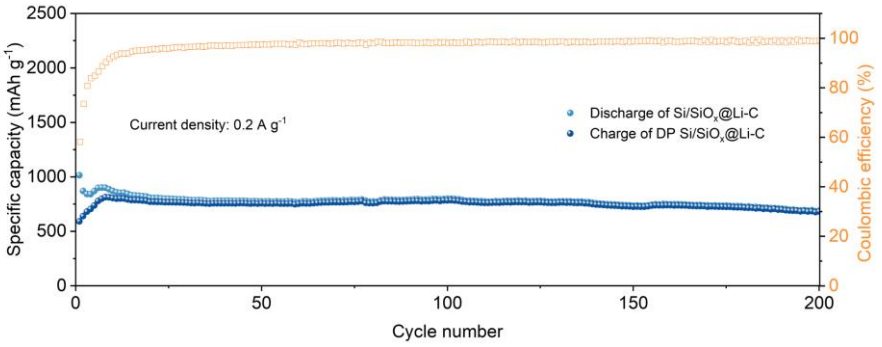

Fig. S12 Cycling performance of DP Si/SiO_x@Li-C at 0.2 A g^{-1}.

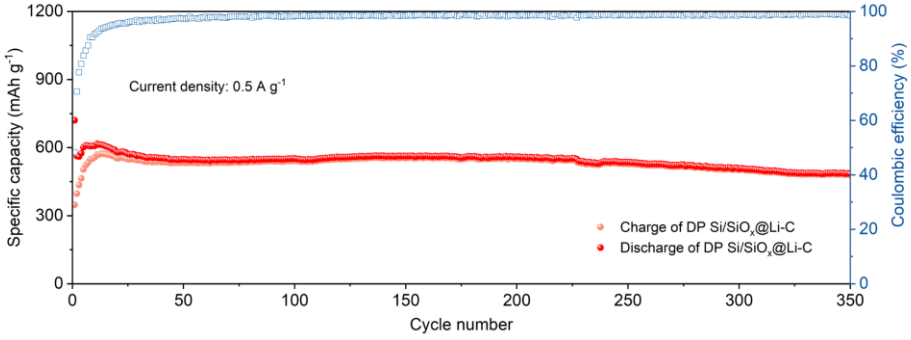

Fig. S13 Cycling performance of DP Si/SiO_x@Li-C at 0.5 A g^{-1}

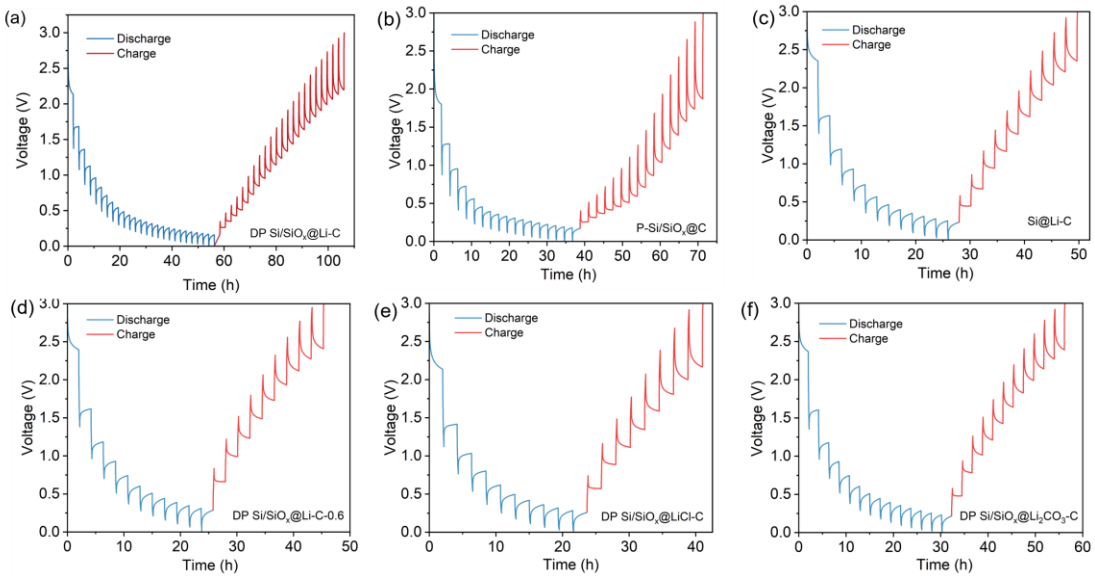

Fig. S14 GITT time-potential distributions of (a) DP Si/SiO_x@Li-C, (b) P-Si/SiO_x@C, (c) Si@Li-C, (d) DP Si/SiO_x@Li-C-0.6, (e) DP Si/SiO_x@LiCl-C, and (f) DP Si/SiO_x@Li_2CO_3-C.

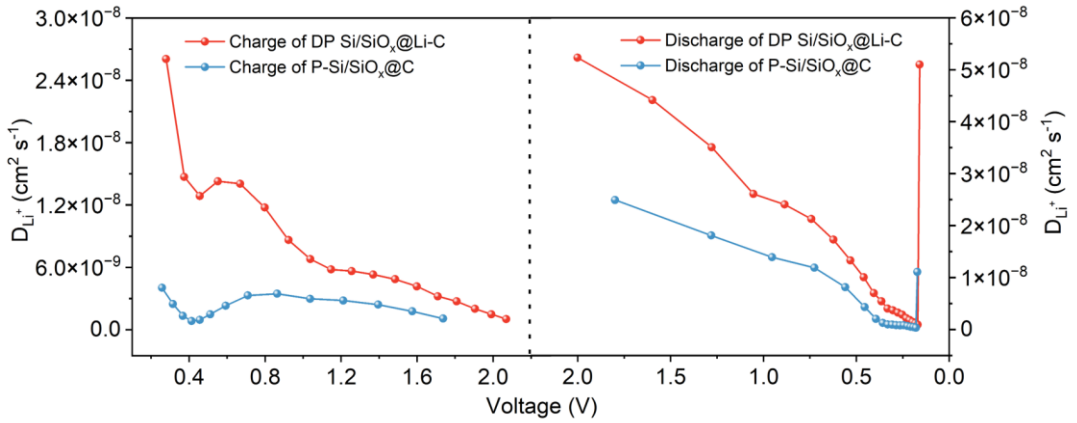

Fig. S15 Ion diffusion coefficients during discharge-charge of DP Si/SiO_x@Li-C and P-Si/SiO_x@C.

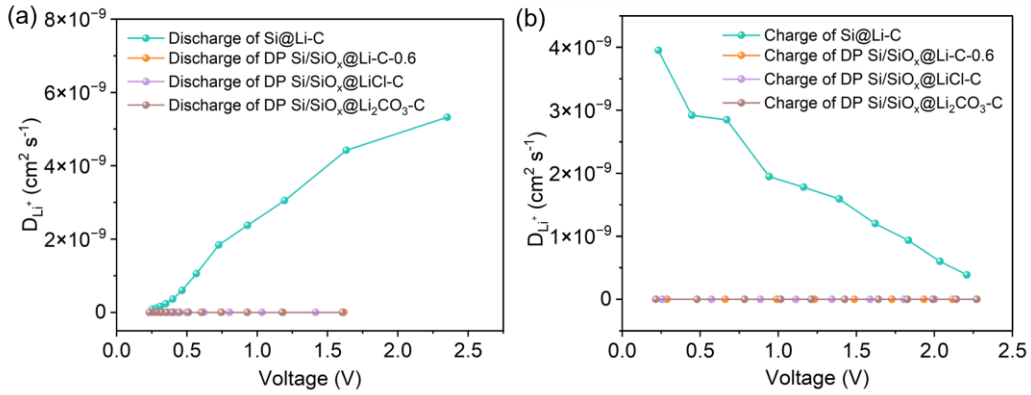

Fig. S16 Ion diffusion coefficients of Si@Li-C, DP Si/SiO_x@Li-C-0.6, DP Si/SiO_x@LiCl-C, and DP Si/SiO_x@Li_2CO_3-C during (a) discharge and (b) charge.

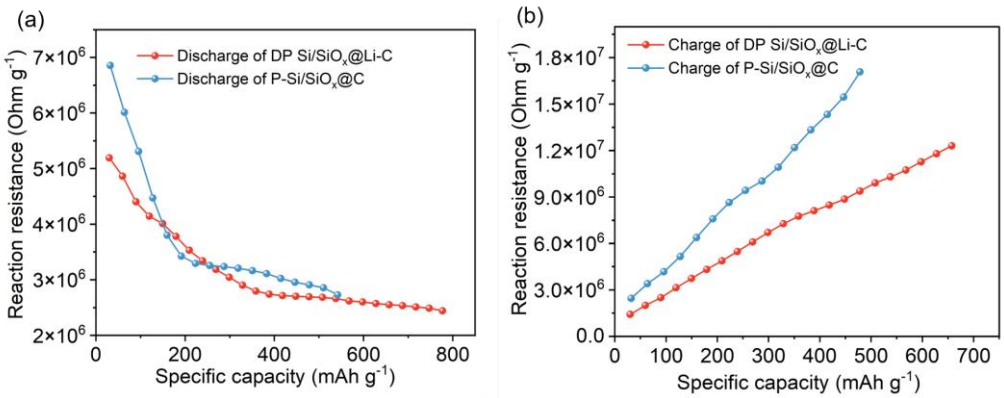

Fig. S17 *In-situ* reaction resistance during (a) discharge and (b) charge of DP Si/SiO_x@Li-C and P-Si/SiO_x@C.

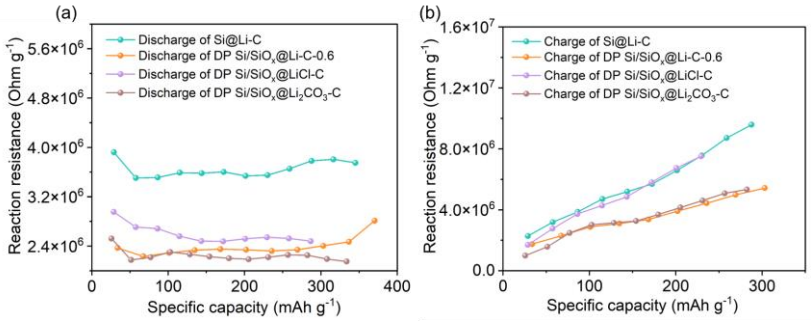

Fig. S18 *In-situ* reaction impedances of Si@Li-C, DP Si/SiO_x@Li-C-0.6, DP Si/SiO_x@LiCl-C, and DP Si/SiO_x@Li_2CO_3-C during (a) discharge and (b) charge.

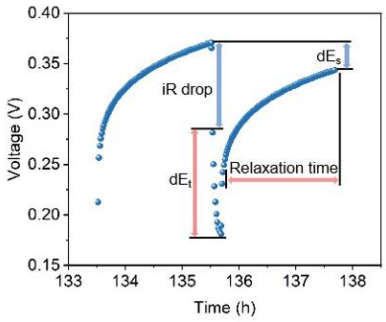

Fig. S19 Illustration of *IR* drop, *dEs*, and *dEτ*.

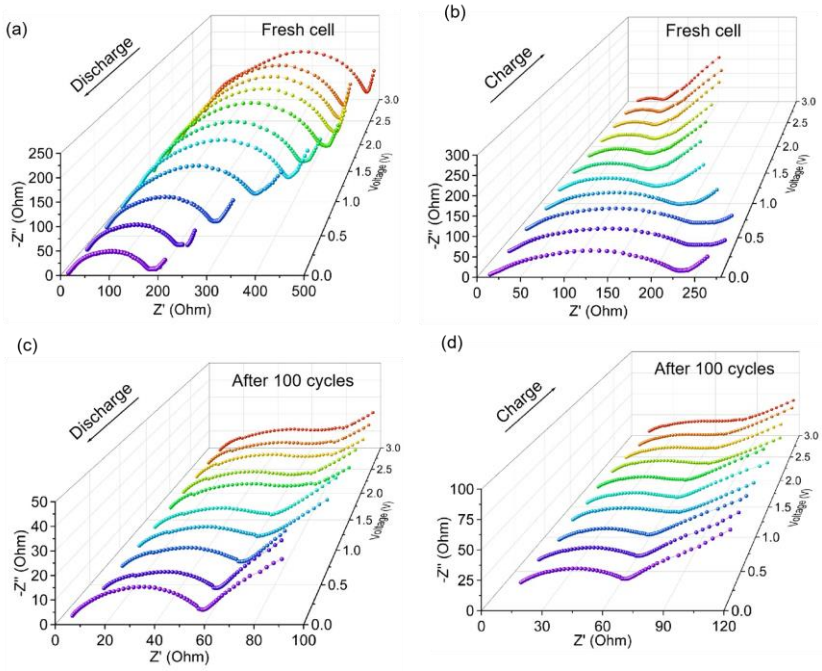

Fig. S20 (a,b) *In-situ* impedance spectra of DP Si/SiO_x@Li-C-based fresh LIBs at different discharge-charge voltage. (c,d) *In-situ* impedance spectra of the battery after 100 cycles at 0.1 A g^{-1} at different discharge-charge voltage.

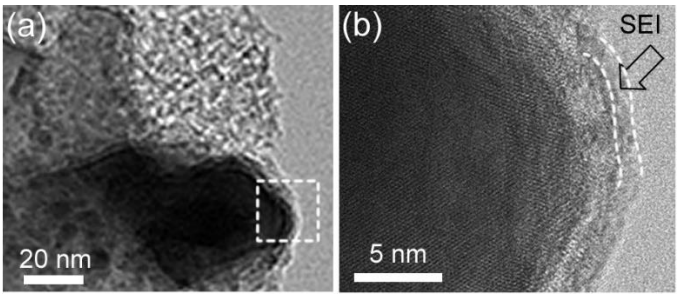

Fig. S21 (a,b) HRTEM images of DP Si/SiO_x@Li-C after 5 cycles at 0.1 A g^{-1}.

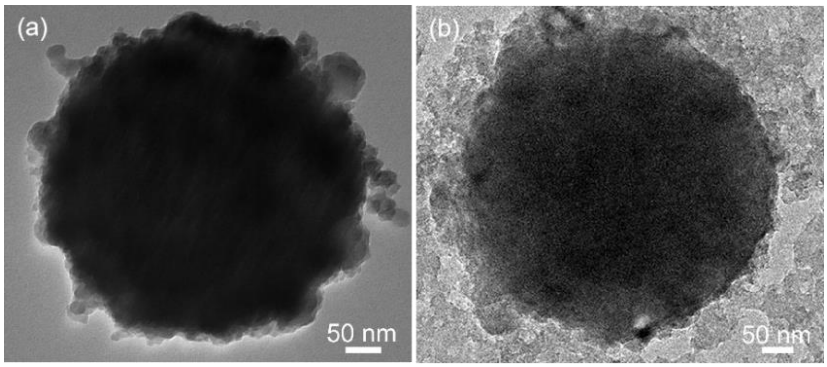

Fig. S22 TEM images of (a) pristine and (b) lithiated DP Si/SiO_x@Li-C spheres.

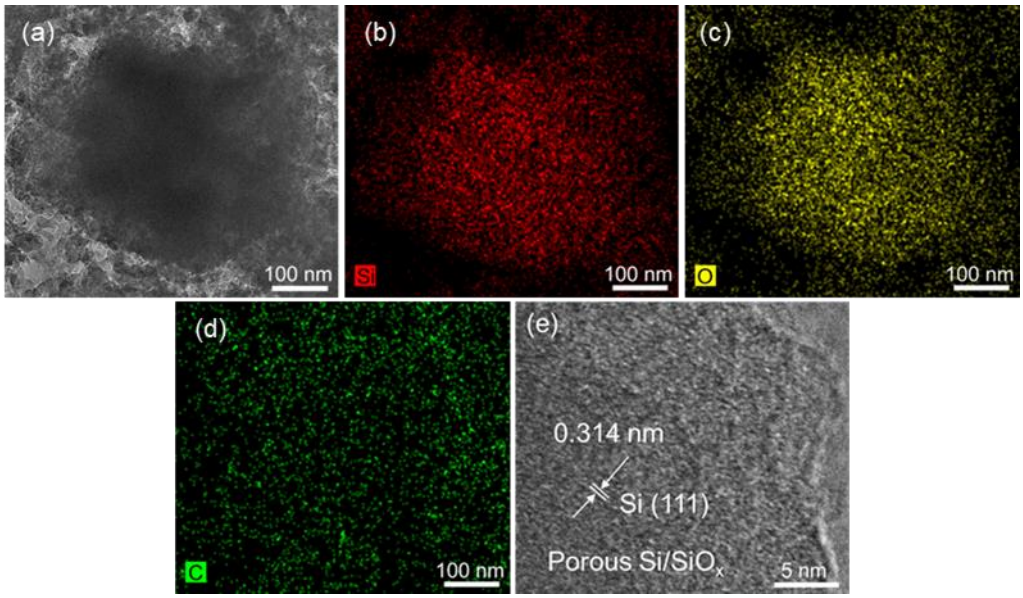

Fig. S23 (a) TEM and (b-d) mapping images of the DP Si/SiO_x@Li-C after cycling 100 times at 0.1 A g^{-1}. (e) HRTEM image.

Table S1. Comparison of the electrochemical performance of some Li-ion battery anodes.

Anodes	Synthesis method	Initial CE (%)	Current density (A g^{-1})	Capacity (mAh g^{-1})	Cycle number	Ref.
C-SiO_x/C	Polymerizing /interfusing	80.7	0.09	836	500	[1]
Si@mesocarbon-microbeads	Magnesiothermic reduction	82.0	0.2	421	200	[2]
Si-C	Magnesiothermic reduction	58.7	0.1	769	31	[3]
SiO_x@Gr/artificial graphite	Electrochemical exfoliation/coating	72.1	0.37	400	50	[4]
Si/C-2	Magnesiothermic reduction	99.0	0.5	300	200	[5]
Graphite-Si@pyroprotein	Mixed drying/carbonization	61.9	0.05	400	100	[6]
C-SiO_x@Si/rGO	Modified Hummers method	60.9	1	925	100	[7]
Porous-Si/C	Magnesiothermic reduction	84.0	0.06	624	120	[8]
Si/carbon nanorod	Evaporation-induced method	46.4	0.1	600	100	[9]
MSi@SiO_x⊂rGO	Modified Hummers method	88.8	1	836	1000	[10]
Nanoporous Si/graphite	Solution-chemical dealloying	62.5	0.5	328	100	[11]
Si CNFs-200	Electrospinning	79.6	0.1	536	100	[12]
Si@C	Ball milling/spray drying	58.8	0.1	402	100	[13]
DP Si/SiO_x@Li-C	Magnesiothermic reduction	66.4	0.1	810	100	This work

References

1 G. Li, L. B. Huang, M. Y. Yan, J. Y. Li, K. C. Jiang, Y. X. Yin, S. Xin, Q. Xu, Y. G. Guo, *Nano Energy*, 2020, **74**, 104890.

2 J. T. Du, J. K. M, Z. T. Liu, W. C. Wang, H. N. Jia, M. X. Zhang, Y. Nie, *Mater. Lett.*,

2022, **315**, 131921.

3 L. F. Guo, S. Y. Zhang, J. Xie, D. Zheng, Y. Jin, K. Y. Wang, D. G. Zhuang, W. Q. Zheng, X. B. Zhao, *Int. J. Miner. Metall. Mater.*, 2020, **27**, 515-525.

4 L. Lee, Wang, W. T. A. Ran, J.-H. Lee, S. M. Hwang, Y.-J. Kim, *Chem. Eng. J.*, 2022, **442**, 136166.

5 J. Zhang, S. Zuo, Y. Q. Wang, H. H. Yin, Z. Q. Wang, J. Wang, *J. Power Sources*, 2021, **495**, 229803.

6 S. M. Cho, J. Yoon, Y. S. Yun, H.-J. Jin, *ACS Appl. Energy Mater.*, 2022, **5**, 15538-15547.

7 T. Meng, B. Li, Q. S. Wang, J. N. Hao, B. B. Huang, F. L. Gu, H. M. Xu, P. Liu, Y. X. Tong, *ACS Nano,* 2020, **14**, 7066-7076.

8 J. H. Wang, C. H. Chuang, P. W. Chi, T. Paul, P. Chandan, K. W. Yeh, C. C. Chang, S. P. Prakoso, Y. C. Chiu, M. K. Wu, *ACS Appl. Nano Mater.,* 2023, **6**, 12578-12587.

9 X. R. Li, H. P. Su, C. Ma, Y. C. Cong, J. Wang, H. Z. Lin, Y. Z. Shang, H. L. Liu, *Mater. Lett.*, 2022, **324**, 132636.

10 S. Q. Ou, C. Liu, R. G. Yang, W. J. Fan, Z. Z. Xie, B. Li, T. Meng, C. J. Zou, D. Shu, Y. X. Tong, *Energy Storage Mater.*, 2024, **73**, 103814.

11 Y. B. Liu, X. Y. Liu, Y. L. Zhu, J. W. Wang, W. W. Ji, X. Z. Liu, *Energy Fuels*, 2023, **37**, 4624-4631.

12 X. H. Li, X. X.Wang, J. J. Li, G. Liu, D. C. Jia, Z. L. Ma, L. Zhang, Z. Peng, X. Y. Zhu, *Electrochem.Commun*., 2022, **137**, 107257.

13 S. Y. Zhang, J. Xie, C. Wu, X. B. Zhao, *Int. J. Electrochem. Sci*., 2020, **15**, 6582-6595.